Hemispheric asymmetry of the premidnight aurora associated with the dawn-dusk component of the interplanetary magnetic field

Liou, K.[1], and E. J. Mitchell[1]
The Johns Hopkins University Applied Physics Laboratory, Laurel, Maryland 20723, USA

Main points:

- Hemispheric auroral asymmetry associated with IMF B_y is studied
- Premidnight auroras in the Northern Hemisphere are more intense for negative than positive IMF B_y
- An opposite effect is found in the Southern Hemisphere

Keywords: premidnight aurora, north-south asymmetry, TIMED/GUVI

Abstract. It has been known for decades that the nightside aurora in the Northern Hemisphere tends to be brighter when the interplanetary magnetic field (IMF) measured at Earth has a dawnward (negative *y*) component compared to a duskward (positive *y*) component. This asymmetric response to the polarity of IMF B_y has been explained by an inter-hemispheric current flowing out of the Northern Hemisphere (NH) due to a non-uniform "penetration" of IMF B_y onto the magnetotail. If such a hypothesis is correct, it should predict a brighter aurora in the nightside Southern Hemisphere (SH) for positive IMF B_y than negative IMF B_y. Here we investigate this hypothesis using TIMED/GUVI data. The present study not only reproduces the result previously found in NH, but also shows an opposite change to its northern hemispheric counterpart in SH in response to the different IMF B_y polarity. When comparing north to south, for negative IMF B_y, the premidnight auroral energy flux is greater in NH than that in SH. The result becomes opposite for positive IMF B_y. This result is consistent with the hypothesis of the existence of an inter-hemispheric field aligned current.

1. Introduction

There is little doubt that the north-south (z) component of the interplanetary magnetic field (IMF) in Geocentric Solar Magnetospheric (GSM) coordinate system is the major driver of the magnetospheric convection and geomagnetic activity. When the IMF is purely southward, the magnetotail structure is nearly dawn-dusk symmetric, which is evidenced by the two-cell convection pattern seen in the ionosphere. When the dawn-dusk (y-) component of the IMF (IMF B_y) is finite, a dawn-dusk asymmetry can be introduced. At the dayside magnetopause, the y-component of IMF controls the azimuthal location where magnetic merging takes place (Zhou et al., 2000; Newell et al., 2007), as predicted by the anti-parallel merging model (Crooker, 1979). After magnetic field merging, the field tension and the solar wind drag can bring newly opened field lines to the opposite dawn-dusk sector. This introduces dawn-dusk asymmetries in the magnetotail configuration (e.g., Kaymaz et al., 1994), resulting in dawn-dusk asymmetries in the high-latitude electrodynamics, such as ionospheric convection (e.g., Ruohoniemi and Greenwald, 1995), transpolar cap (theta) arcs (Frank et al., 1982, 1986; Cumnock et al., 1997; Chang et al., 1998), dayside auroras (Murphree et al., 1981; Vo and Murphree, 1995; Liou et al., 1998), substorm azimuthal onset location (Liou and Newell, 2010; Østgaard et al., 2011) and substorm expansion (Liou and Ruohoniemi, 2006; Liou et al., 2006).

The y-component of IMF not only introduces dawn-dusk asymmetries in the magnetosphere and ionosphere, it also affects the nightside aurora, mainly in the premidnight sector where discrete auroras dominate (e.g., Newell et al., 2009). Liou et al. (1998) perform statistical analysis of global images of northern auroras acquired from the UltraViolet Imager (UVI) on board the Polar spacecraft. Based on 4-months of data (~10000 images), they find that the nightside (20 – 01 MLT) auroral power shows an increase with the IMF clock angle (the angle of the projected IMF on the GSM y-z plane with respect to the z axis). However, the increase is not

symmetric; the increase is larger for duskward IMF B_y (negative IMF B_y) than for dawnward IMF B_y (positive IMF B_y). Shue et al. (2001) revisit this finding with a larger (~2 years) dataset from Polar UVI, also in the Northern Hemisphere, and showed that nightside auroral power is greater for IMF $B_y < 0$ than for IMF $B_y > 0$, and more pronounced when the southward IMF is larger. They attribute such an asymmetric response of the nightside auroras, presumably mostly auroral arcs, to an extra B_y component in the magnetotail associated with IMF B_y "penetration" (e.g., Cowley et al., 1981; Newell et al., 1995; Wing et al., 1995). The IMF B_y penetration into the closed magnetotail is nonuniform. The penetration efficiency is found to be ~0.8 at the geosynchronous orbits (Wing et al., 1995) and ~0.5 in the mid-tail plasma sheet from -30 to -10 R_E (Lui, 1984), indicating that the penetration is more efficient closer to the Earth. Stenbaek-Nielsen and Otto (1997) argue that such a nonuniform extra B_y distribution in the closed tail infers an inter-hemispheric field-aligned current flowing out of the northern hemispheric polar region into the southern hemispheric polar region (see Figure 1). The inferred inter-hemispheric field-aligned current is consistent with the observed non-conjugate auroral arcs they report.

Previous airplane-based and ground-based observations of auroral images have shown that auroral forms may not be conjugate (e.g., Stenbaek-Nielsen et al., 1972; Davis and Stenbaek-Nielsen, 1974; Sato et al., 1998, 2005). However, these observations are sporadic and localized; this means that the observations focus on small auroral structures that may be associated with ionospheric plasma instability. The nonzero IMF B_y-induced magnetotail configuration asymmetry is a global-scale phenomenon. Thus, studies of nightside aurora from both hemispheres in a statistical manner are required to provide a rigorous test of the hypothesis of the existence of an inter-hemispheric field aligned current. The purpose of this study is to provide a stronger argument for the asymmetric response of the nightside aurora to IMF B_y.

2. Data and Data Processing

In this study, we use auroral images acquired by the Global Ultraviolet Imager (GUVI) (Paxton et al., 1999; Christensen et al., 2003) on-board the Thermosphere, Ionosphere, Mesosphere, Energetics and Dynamics (TIMED) spacecraft from February, 2002 to November, 2007. GUVI is a (mirror) scanning spectrometer in the far ultraviolet (~120 – 180 nm) wavelength. Auroral emissions are scanned horizon-to-horizon while crossing the polar region. Due to the "low" inclination (74°) and 625 km near-circular sun-synchronous orbit of the TIMED spacecraft, GUVI takes about 1/3 – ½ of the auroral oval during each crossing with a cadence of 90 minutes. Because of single satellite observations, the north and south auroral regions are not observed simultaneously. Therefore, the present analysis and result comparison are statistical in nature. For the present analysis, the total number of images is 28,774 and 29,742 for the Northern and Southern Hemisphere, respectively.

The acquired auroral emissions are converted to physical quantities, such as the energy flux and characteristic energy of precipitating electrons. The method for deriving the energy flux and error analysis is given by Zhang and Paxton (2008) and Liou et al. (2011), respectively. The original Earth disk images have different spatial resolution, with a finer resolution toward the nadir from the limb. We re-binned the images to nearly uniform grids (1° in latitude and an equal length (~110 km) in longitude) in the Altitude Adjusted Corrected Geomagnetic Coordinates Magnetic (AAGCM) coordinates (Baker and Wing, 1999).

The IMF data is based on high resolution (HRO) OMNI data (1-minute cadence) provided by NASA's Space Physics Data Facility (SPDF). The OMNI/HRO data sets provide the solar wind plasma and IMF measurements from multiple spacecraft measurements in the solar wind at the subsolar bow shock using minimum variance algorithms developed by Weimer and King (2008). For the present analysis, we add an additional 45 minutes to allow for propagation through the bow shock, magnetosheath, and dayside magnetosphere to the magnetotail (Tenfjord et al.,

2017). Because it takes ~10 min for GUVI to cross the oval, we average the IMF data by a 10-min time window centered at the image center time. Different delay times (30 – 60 minutes) and average time windows (up to 60 minutes) have been tested and found to have similar results. The GSM coordinate system is used throughout the study to represent the three components of IMF.

3. Statistical Results

To compare auroral images for different IMF B_y polarity, we sort the data into bins based on the IMF B_y values from OMNI/HRO. We also require IMF $B_z < -1$ nT. Such a requirement is consistent with the IMF penetration through magnetic merging. To avoid a possible IMF B_x effect (Shue et al., 2002; Reistad et al., 2014), we further limit the data set to those with an absolute value of IMF $B_x < 2$ nT. It is well established that nightside auroras are suppressed in sunlight (e.g., Newell et al., 1996; Liou et al., 1997, 2001) and the nightside auroral energy flux increases with increasing solar zenith angles (Liou et al., 2001). Therefore, we further require large solar zenith angles (>108°) to make sure that auroras are observed in darkness.

Figures 2 and 3 show the averaged auroral energy flux for negative IMF B_y ($B_y < -2$ nT) and positive IMF B_y ($B_y > 2$ nT), respectively, for the Northern (left) and Southern (right) Hemispheres. Although we started with ~30k images for each hemisphere, the actual number of images of the Earth's disk contributing to the composite auroral images for the following analysis are small (around hundreds). Comparing the nightside auroras in the Northern Hemisphere (NH) with different IMF B_y polarity, one can see that the auroral energy flux in NH premidnight sector is larger for negative IMF B_y than for positive IMF B_y. This is consistent with previous studies using global FUV auroral images from Polar (Liou et al., 1998; Shue et al., 2001). In contrast to the Northern Hemisphere, the comparison is opposite in the Southern Hemisphere (SH) – the auroral energy flux in the premidnight sector is larger for positive IMF B_y than for negative IMF B_y. When comparing NH with SH, the auroral energy flux in the NH premidnight sector is larger

than its SH counterpart for negative IMF B_y. For positive IMF B_y, auroral energy flux is larger (but only slightly) in the nightside SH than NH.

To provide a quantitative context, we calculate the energy flux averaged over each hourly sector for both hemispheres and both IMF B_y polarities. The hourly sector is defined as the "pie-shape" area between the beginning and end of each hour and above 60° MLat. The results are shown in Figure 4. Figures 4(a) and 4(b) show nightside (18 – 06 MLT) auroral particle energy flux in the Northern and Southern Hemisphere, respectively. In the Northern Hemisphere, the energy flux in the premidnight sector (18 – 24 MLT) is larger for negative (filled circles) than for positive (open circles) IMF B_y, whereas the relationship is reversed in the Southern Hemisphere. Figures 4(c) and 4(d) compare the NH and SH hourly-sector auroral energy flux for the same IMF B_y conditions. They are simply reordered and redrawn from Figures 4(a) and 4(b) results. One can see that the auroral energy flux clearly dominated in the Northern Hemisphere for IMF $B_y < -2$ nT. The north-south difference ranges from 15% at 19 MLT to 20% at 23 MLT. In contrast, the auroral energy flux dominated in the Southern Hemisphere for IMF $B_y > 2$ nT. The south-north difference ranges from ~11% at 19 MLT to ~34% at 23 MLT.

There is an interesting point of Figure 4, namely that for positive B_y, the energy fluxes in SH are larger not only in the pre-midnight sector, but also in the post-midnight sector until 6 MLT. The difference is clear even taking the error bars into account. It is well known that auroras that occur in the postmidnight sector are mainly diffuse (Newell et al., 2009) and are associated with pitch-angle scattering of hot central plasma sheet electrons (e.g., Thorne et al., 2010). We will not address this as the present study focuses on auroras associated with field-aligned currents.

Before we can attribute the north-south asymmetry in the auroral energy flux to the IMF B_y polarity, we need to check the IMF B_z conditions for the data sets that are selected for the analysis. After all, the southward component of the IMF is the major parameter that controls the

solar wind-magnetosphere coupling through magnetic merging/reconnection. Figures 5(a) and 5(b) show the normalized distribution of IMF B_z for northern and southern hemispheric events for (a) IMF $B_y < -2$ nT and (b) IMF $B_y > 2$ nT. For both IMF B_y polarities, the distribution of IMF B_z is almost identical for the northern and southern hemispheric events. The averaged B_z values for northern (southern) hemispheric events are nearly identical: -3.01 (-2.90) and -2.81 (-2.87) nT for IMF $B_y < -2$nT and IMF $B_y > 2$nT, respectively. Therefore, we can rule out the effect of IMF B_z to the observed asymmetry.

Another way to test the consistency of the IMF B_y effect is to check for a relationship between the auroral energy flux and the IMF B_y component. Figure 6 (bottom panel) shows the averaged auroral energy flux in the premidnight sector of the NH (blue) and SH (red) as a function of the IMF B_y component. The histograms of the associated IMF B_y and hemispheres are plotted on the top panel. We do not see a significant difference in the sample distributions. The averaged positive (negative) IMF B_y value is 3.05 nT (-3.14 nT) for the northern hemispheric events and 2.91 nT (-2.94 nT) for the southern hemispheric events. It is shown that the averaged energy flux increases with increasing IMF $|B_y|$ for both hemispheres. However, there is a marked difference in the rate of the increase. In the NH, the increase rate is higher for IMF $B_y < 0$ than for IMF $B_y > 0$; however, in the SH, the increase rate becomes higher for IMF $B_y > 0$ than for IMF $B_y < 0$. Figure 6 also shows that for the same IMF B_y polarity, there is north-south asymmetry in the auroral energy flux. The averaged auroral energy flux is higher in the NH than in the SH for IMF $B_y < 0$, whereas it is higher in the SH than in NH for IMF $B_y > 0$. This result further supports the result shown in Figures 2 and 3.

4. Discussion

We have conducted a statistical study of the north-south auroras in the form of particle precipitating energy flux under positive and negative IMF B_y conditions. The particle

precipitating energy flux is inferred from FUV spectrograph images of the Earth disk acquired by GUVI. It is well known that a finite IMF B_y component is prone to produce a dawn-dusk asymmetry in the magnetosphere/ionosphere such as a dawn-dusk displacement of the auroral oval (Holzwarth and Meng, 1984) and the cusp (Newell et al., 1989), and a dawn-dusk asymmetry in the convection flow pattern (Ruohoniemi and Greenwald, 1995). Here we have focused only on the aurora in the dusk-to-midnight (18 – 24 MLT) sector, and especially its north-south asymmetry. The present study not only reproduced previous results from a completely different data set, Polar UVI (Liou et al., 1998; Shue et al., 2001), but also clearly shows a statistical north-asymmetry in the premidnight auroral intensity. Under southward IMF conditions (IMF $B_z < 1$ nT), the average auroral energy flux in the northern hemispheric premidnight sector (18 – 24 MLT) is larger for IMF $B_y < 0$ than for IMF $B_y > 0$. This IMF B_y dependency becomes opposite in the Southern Hemisphere.

The direct association of the IMF B_y component to the aurora is not straightforward, as the auroral variability is complex. Since the premidnight sector auroral power increases linearly with the magnitude of the negative *z*-component of IMF (Liou et al., 1998), one may argue that the asymmetric response to the IMF B_y component is due to the asymmetric distribution of the IMF B_z component. However, this is not supported by our result. As shown in Figure 5, the distributions of IMF B_z for both positive and negative IMF B_y conditions and for both hemispheres are similar. Furthermore, in the Southern Hemisphere, the auroral power is significantly larger (~40% around midnight) for positive than negative IMF B_y. However, the averaged values of IMF B_z for the positive and negative IMF B_y conditions are nearly the same (-2.87 vs -2.90). Therefore, we can rule out the IMF B_z effect. Past statistical studies of auroras in one hemisphere have suggested possible north-south asymmetries in association with the IMF orientation in the *x* (Liou et al., 1998; Shue et al., 2002; Reistad et al.,, 2014) and *y* components

(Liou et al., 1998; Shue 2001), and solar illumination (e.g., Newell et al., 1996; Liou et al., 1997, 2001). The condition of solar illumination clearly shows a north-south asymmetry. Indeed, the suggested solar illumination has, to some extent, been confirmed statistically (Ohtani et al., 2009). In this study, we limited the solar zenith angle to greater than 108°. As shown in Liou et al. (2011), the nightside (21 – 03 MLT) auroral energy flux increases with the solar zenith angle and approaches the peak around 110°. Therefore, we can also rule out the solar illumination effect. It has been reported that the dayside (13 – 18 MLT) auroral power in the Northern Hemisphere tends to be larger for a negative IMF B_x-component (Shue et al., 2002). Later, using data from the Wide-band Imaging Camera on the IMAGE satellite, Reistad et al. (2014) confirmed that such an IMF B_x effect can introduce a north-south asymmetry in the dusk aurora. They found statistically that the northern aurora in the 15 – 19 MLT sector is brighter during negative IMF B_x, whereas the southern aurora in the 16 – 20 MLT sector is brighter during positive IMF B_x. This IMF B_x effect has been explained in the context of dayside magnetic merging (Reistad et al., 2014). To avoid such an effect, we have limited the data for small IMF B_x absolute value (< 2 nT) and focused on the nightside aurora.

The effect of a finite IMF B_y-component on the nightside aurora is first illustrated by Stenbaek-Nielsen et al. (1972) in their conjugate auroral observations using airborne allsky imagers near the College, Alaska magnetic meridian. They propose an inter-hemispheric field-aligned current to explain the north-south auroral intensity asymmetry that they observe. The inter-hemispheric field aligned current is generated by partial penetration of IMF B_y onto the closed magnetosphere. Since the penetration is not uniform, being more efficient close to the Earth (see Figure 1), the extra non-uniform B_y component in the magnetotail can induce a field-aligned current, flowing out of the Northern Hemisphere when IMF B_y is negative, as predicted by the Ampere's law $\boldsymbol{j} \sim \nabla \times \boldsymbol{B}$ $(= -z\, \partial B_y/\partial x)$. Such a field-aligned current is expected to result in

auroral arcs in the northern hemisphere only, producing a north-south asymmetry in the occurrence and brightness of auroral arcs. On the other hand, when IMF B_y is positive, the situation becomes opposite, i.e., more intense auroral arcs are expected in the Southern Hemisphere.

The extra B_y component in the magnetotail is generally interpreted in terms of open magnetosphere concept (Cowley, 1981), in which the *y*-component of the IMF is added into the magnetically closed field lines of the magnetosphere through the merging-reconnection process. Newell et al. (1995) proposed a "replenish" merging field model to address the IMF B_y penetration onto closed dayside magnetic field lines. In this model, an extra B_y component results from an action of Earth's magnetic field to fill recently removed nearby closed fields, through merging. More recently, Tenfjord et al. (2015), using magnetohydrodynamics simulation, propose a model based on magnetic tension and azimuthal flow asymmetry between the two hemispheres. Browett et al. (2017) address the issue of IMF B_y penetration into the neutral sheet by analyzing the response time and penetration efficiency. They conclude that their result in the response time is consistent with the convection-driven process (Cowley, 1981). While the mechanism for penetration of the IMF B_y component is still not clear, the existence of an extra B_y component in the magnetosphere has been observed by many researchers. The ratio of the plasma sheet B_y to the IMF B_y field increases from 21% at $X_{GSM} > 150\ R_E$ (Tsurutani et al., 1984) to 50% between -10 and -30 R_E (Lui, 1986), to ~80% at the geosynchronous orbits (Wing et al., 1995). While other studies have shown a large variability in the penetration efficiency (e.g., Kaymaz et al., (1994)), Petrukovich (2011) shows the local B_y component in the magnetosphere can be fitted linearly with IMF B_y component, using 11-year worth of Geotail measurements.

Although the concept of "penetration" of IMF B_y onto the magnetosphere in interpreting the observed north-south asymmetry as shown in the present study is plausible, the proposed inter-

hemispheric field-aligned current has not been observed. On the other hand, the present study may provide support for the existence of inter-hemisphere currents. The existence of inter-hemispheric field-aligned current would generate auroras in the outgoing hemisphere only and cause north-south asymmetry in the auroral intensity. Therefore, for IMF $B_y < 0$, the current will flow out of the Northern Hemisphere and generate aurora in that hemisphere only. On the other hand, for IMF $B_y > 0$, the current will flow out of the Southern Hemisphere and generate aurora in that hemisphere only. This reasoning is supported by the present study results showing a larger mean energy flux in the hemisphere where the current is flowing out for positive or negative IMF B_y (see Figures 4(c) and 4(d)). Of course, one cannot exclude possibilities that other mechanisms exist that are responsible for the observed asymmetry in the north-south auroras. For example, it has been reported that a non-zero B_y component can have significant effect on particle dynamics in the magnetotail (e.g., Zhu and Parks, 1993). For a zero B_y component, particle orbits in the current sheet in the phase space are symmetric about the $z = 0$ (equatorial) plane. When a non-zero B_y is introduced, charged particles, after energized by and escaped from the current sheet, tend to be ejected toward one hemisphere than the other depending on the sign of B_y (Zhu and Parks, 1993). Based on their theoretical calculation of particle orbits in a modeled current sheet, they found that negatively (positively) charged particles, after acceleration by the current sheet, tend to be ejected toward the Northern (Southern) Hemisphere for a negative B_y component and toward the Southern Hemisphere for a positive B_y component in the current sheet. While the ejected charged particles can be the current carrier and form an inter-hemispheric current in the same direction as predicted by the IMF B_y penetration hypothesis, it is not clear how significant the "scattering" (by the current sheet) process is in the north-south auroral asymmetry. Furthermore, such scattered and precipitated particles are likely to be associated with diffuse auroras, which are known to occur predominately in the midnight-to-dawn sector (Newell et al.,

2009), and are not the major contributor of the aurora in the premidnight sector.

It is well known that auroral breakups occur mainly in this dusk-to-midnight sector (e.g., Liou, 2010). Thus, the finding that the auroral energy flux in the premidnight sector in the Northern Hemisphere is larger for negative IMF B_y than positive IMF B_y components may suggest that substorms are more frequent during intervals of negative IMF B_y than positive IMF B_y. A quick test of this hypothesis can be done with a list of 2003 auroral breakup events identified by Liou (2010) using the Polar UVI northern hemispheric image data. Here we calculate the average and median values of the 45-min averages of the IMF B_y component. It is found that the average IMF B_y value is -0.01 nT and the median IMF B_y value is 0.00 nT. The average time period has no significant impact on these values (tested 15, 30, 45, and 60 minutes). Therefore, we can rule out this possibility.

5. Summary and Conclusions

The main results of the present study are summarized as follows. (1) Auroral energy flux in the Northern Hemisphere is larger for IMF $B_y < 0$ than for IMF $B_y > 0$, whereas the relation is opposite in the Southern Hemisphere – auroral energy flux is larger for IMF $B_y > 0$ than for IMF $B_y < 0$. (2) For IMF $B_y < 0$, auroral energy flux is larger in the Northern Hemisphere than in the Southern Hemisphere, whereas the effect is opposite for IMF $B_y > 0$. This may infer an inter-hemispheric field-aligned current on auroral field lines. These findings are consistent with the predictions of the "penetration" of IMF B_y component. Because of the bimodal distribution of IMF B_y, this IMF B_y-associated north-south asymmetry in the premidnight aurora is expected to cause an asymmetry in the electrodynamics of the ionosphere and their interactions with the thermosphere. Further studies of this effect would help model the ionospheric/thermospheric system as a whole more precisely.

Acknowledgements

We acknowledge the use of the NASA/GSFC's Space Physics Data Facility's OMNIWeb (or CDAWeb or ftp) service and OMNI data. The GUVI instrument was designed and built by The Aerospace Corporation and the Johns Hopkins University. The Principal Investigator is Andre B. Christensen and the Co-PI is Larry J. Paxton. The GUVI data reporeted herein are available through the TIMED/GUVI website at guvitimed.jhuapl.edu. This study was supported by NSF 1408812/121167 and 1743118 grants to the Johns Hopkins University Applied Physics Laboratory.

References

Browett, S. D., R. C. Fear, A. Grocott, and S. E. Milan (2017), Timescales for the penetration of IMF *By* into the Earth's magnetotail, *J. Geophys. Res. Space Physics*, 122, 579–593, doi:10.1002/2016JA023198

Chang, S.-W., et al. (1998), A comparison of a model for the theta aurora with observations from Polar, Wind, and SuperDARN, *J. Geophys. Res.*, *103*(A8), 17367–17390, doi:10.1029/97JA02255.

Christensen, A. B. et al. (2003), Initial observations with the Global Ultraviolet Imager (GUVI) in the NASA TIMED satellite mission, *J. Geophys. Res*., *108*(A12), 1451, doi:10.1029/2003JA009918.

Cowley, S. W. H. (1981), Magnetospheric asymmetries associated with the y-component of the IMF, *Planet. Space Sci.*, *29*, 79.

Crooker, N. U. (1979), Dayside merging and cusp geometry, *J. Geophys. Res*., *84*, 951.

Cumnock, J. A., J. R. Sharber, R. A. Heelis, M. R. Hairston, and J. D. Craven (1997), Evolution of the global aurora during positive IMF Bz and varying IMF By conditions, *J. Geophys. Res.*, *102*(A8), 17489–17497, doi: 10.1029/97JA01182.

Davis, T, N. and H, C. Stenbaek-Nielsen (1974), Conjugate break-up, *Mem. Nat. Inst. Polar Res. Spec. Issue Jpn.*, 3, 4.Frank, L. A., Craven, J. D., Burch, J. L. and Winningham, J. D. (1982), Polar views of the Earth's aurora with Dynamics Explorer. Geophys. Res. Lett., 9: 1001-1004. doi:10.1029/GL009i009p01001

Frank, L. A., J. D. Craven, J. L. Burch, and J. D> Winningham (1982), Polar views of the Earth's aurora with Dynamics Explorer, Geophys. Res., Lett., 9, 1001-1004, doi:10.1029/GL009i009p01001.

Frank, L. A., et al. (1986), The theta aurora, *J. Geophys. Res.*, 91(A3), 3177–3224, doi:10.1029/JA091iA03p03177

Frey, H. U., S. B. Mende, V. Angelopoulos, and E. F. Donovan (2004), Substorm onset observations by IMAGE-FUV, *J. Geophys. Res., 109*, A10304, doi:*10.1029/2004JA010607*.

Holzworth, R. H., and C.-I. Meng, Auroral boundary variations and the interplanetary magnetic field, *Planet. Space Sci*., *32*, 25, 1984.

Kaymaz, Z., G. L. Siscoe, J. G. Luhmann, R. P. Lepping, and C. T. Russell (1994), Interplanetary magnetic field control of magnetotail magnetic field geometry: IMP 8 observations, *J. Geophys. Res.*, *99*(A6), 11113–11126, doi:10.1029/94JA000300.

Liou, K. (2010), Polar Ultraviolet Imager observation of auroral breakup, *J. Geophys. Res*., *115*, A12219, doi:10.1029/2010JA015578.

Liou, K., and P. T. Newell (2010), On the azimuthal location of auroral breakup: Hemispheric asymmetry, *Geophys. Res. Lett.*, *37*, L23103, doi:10.1029/2010GL045537.

Liou, K., and J. M. Ruohoniemi (2006), A case study of relationship between substorm expansion and global plasma convection, *Geophys. Res. Lett.*, *33*, L02105, doi: 10.1029/2005GL024736.

Liou, K., P. T. Newell, C.-I. Meng, M. Brittnacher, and G. Parks (1997), Synoptic auroral distribution: A survey using Polar ultraviolet imagery, *J. Geophys. Res.*, *102*(A12), 27197–27205, doi: . 10.1029/97JA02638.

Liou, K., P. T. Newell, C.-I. Meng, M. Brittnacher, and G. Parks (1998), Characteristics of the solar wind controlled auroral emissions, *J. Geophys. Res.*, *103*(A8), 17543–17557, doi:10.1029/98JA01388.

Liou, K., P. T. Newell, and C.-I. Meng (2001), Seasonal effects on auroral particle acceleration and precipitation, *J. Geophys. Res.*, *106*(A4), 5531–5542, doi:10.1029/1999JA000391.

Liou, K., C.-I Meng, and C.-C. Wu (2006), On the interplanetary magnetic field B_y control of substorm bulge expansion, *J. Geophys. Res.*, 111, A09312, doi: 10.1029/2005JA011556

Liou, K., Y.-L. Zhang, P. T. Newell, L. J. Paxton, and J. F. Carbary (2011), TIMED/GUVI observation of solar illumination effect on auroral energy deposition, *J. Geophys. Res.*, *116*, A09305, doi:10.1029/2010JA016402.

Lui, A. T. (1986), Solar wind influence on magnetotail configuration and dynamics, in *Solar Wind-Magnetosphere Coupling*, edited by Y. Kamide and J. A. Slavin, p. 671, Kluwer, Norwell, Mass..

Murphree, J. S., L. L. Cogger, and C. D. Anger (1981), Characteristics of the instantaneous auroral oval in the 1200–1800 MLT sector, *J. Geophys. Res.*, *86*(A9), 7657–7668, doi:10.1029/JA086iA09p07657.

Newell, P. T., C.-I. Meng, D. G., Sibeck, and R. Lepping (1989), Some low-altitude cusp dependencies on the interplanetary magnetic field, *J. Geophys. Res*., *94*, 8921.

Newell, P. T., C.-I. Meng, K. M. Lyons (1996), Suppression of discrete aurorae by sunlight, *Nature*, *381*, 766.

Newell, P. T., S. Wing, and F. J. Rich (2007), Cusp for high and low merging rates, *Journal of Geophysical Research: Space Physics*, *112*, A9.

Newell, P. T., T. Sotirelis, and S. Wing (2009), Diffuse, monoenergetic, and broadband aurora: The global precipitation budget, *J. Geophys. Res.*, 114, A09207, doi:10.1029/2009JA014326.

Ohtani, S., S. Wing, G. Ueno, and T. Higuchi (2009), Dependence of premidnight field-aligned currents and particle precipitation on solar illumination, *J. Geophys. Res.*, *114*, A12205, doi: 10.1029/2009JA014115.

Østgaard, N., K. M. Laundal, L. Juusola, A. Åsnes, S. E. Håland, and J. M. Weygand (2011),

Inter-hemispherical asymmetry of substorm onset locations and the interplanetary magnetic field, *Geophys. Res. Lett.*, *38*, L08104, doi: 10.1029/2011GL046767.

Paxton, L. J., et al. (1999), Global Ultraviolet imager (GUVI): Measuring composition and energy inputs for the NASA Thermosphere Ionosphere Mesosphere Energetics and Dynamics (TIMED) mission, in Optical Spectroscopic Techniques and Instrumentation fro Atmospheric and Space Research III, edited by Allen M. Larar, Proc. SPIE, 3756, 256-276.

Petrukovich, A. A. (2011), Origins of plasma sheet *By*, *J. Geophys. Res.*, *116*, A07217, doi: 10.1029/2010JA016386.

Reistad, J. P., N. Østgaard, K. M. Laundal, S. Haaland, P. Tenfjord, K. Snekvik, K. Oksavik, and S. E. Milan (2014), Intensity asymmetries in the dusk sector of the poleward auroral oval due to IMF B_x, *J. Geophys. Res*. *Space Physics*, *119*, 9497–9507, doi: 10.1002/2014JA020216.

Ruohoniemi, J. M., and R. A. Greenwald (1995), Observations of IMF and seasonal effects in high-latitude convection, *Geophys. Res., Lett*., *22*, 1121-1124.

Sato, N., T. Nagaoka, K. Hashimoto, and T. Saemundsson (1998), Conjugacy of isolated auroral arcs and nonconjugate auroral breakups, *J. Geophys. Res.*, *103*(A6), 11641–11652, doi:10.1029/98JA00461.

Sato, N., A. Kadokura, Y. Ebihara, H. Deguchi, and T. Saemundsson (2005), Tracing geomagnetic conjugate points using exceptionally similar synchronous auroras, *Geophys. Res. Lett.*, *32*, L17109, doi:10.1029/2005GL023710.

Shue, J.-H., P. T. Newell, K. Liou, and C.-I. Meng (2001), Influence of interplanetary magnetic field on global auroral patterns, *J. Geophys. Res*., *106*(A4), 5913–5926, doi: 10.1029/2000JA003010.

Shue, J.-H., P. T. Newell, K. Liou, C.-I Meng, and S. W. H. Cowley (2002), Interplanetary

magnetic field B_x asymmetry effect on auroral brightness, *J. Geophys. Res.*, *107*(A8), 1197, doi:10.1029/2001JA000229.

Stenbaek-Nielsen, H. C., and A. Otto (1997), Conjugate auroras and the interplanetary magnetic field, *J. Geophys. Res*., *102*(A2), 2223-2232.

Stenbaek-Nielsen, H. C., T. N. Davis, and N. W. Glass (1972), Relative motion of auroral conjugate points during substorms, *J. Geophys. Res.*, *77*(10), 1844–1858, doi:10.1029/JA077i010p01844.

Tenfjord, P., N. Østgaard, K. Snekvik, K. M. Laundal, J. P. Reistad, S. Haaland, and S. E. Milan (2015), How the IMF *By* induces a *By* component in the closed magnetosphere and how it leads to asymmetric currents and convection patterns in the two hemispheres, *J. Geophys. Res. Space Physics*, 120, 9368–9384, doi: 10.1002/2015JA021579.

Tenfjord, P., N. Østgaard, R. Strangeway, S. Haaland, K. Snekvik, K. M. Laundal, J. P. Reistad, and S. E. Milan (2017), Magnetospheric response and reconfiguration times following IMF *By* reversals, *J. Geophys. Res. Space Physics*, 122, 417–431, doi: 10.1002/2016JA023018.

Thorne, R. M., B. Ni, X. Tao, R.B. Horne, N.P. Meredith, Scattering by chorus waves as the dominant cause of diffuse auroral precipitation. Nature 467 (2010). doi:10.1038/nature09467

Tsurutani, B. T., D. E. Jones, R. P. Lepping, E. J. Smith, and D. G. Sibeck (1984), The relationship between the IMF By and the distant tail (150-238 Re) lobe and plasmasheet By fields, *Geophys. Res. Lett.*, *11*(10), 1082–1085, doi: 10.1029/GL011i010p01082.

Vo, H. B., and J. S. Murphree (1995), A study of dayside auroral bright spots seen by the Viking Auroral Imager, *J. Geophys. Res.*, *100*(A3), 3649–3655, doi:10.1029/94JA03138.

Weimer, D. R., and J. H. King (2008), Improved calculations of interplanetary magnetic field phase front angles and propagation time delays, *J. Geophys. Res.*, *113*, A01105, doi:

10.1029/2007JA012452.

Wing, S., Newell, P. T., Sibeck, D. G., & Baker, K. B. (1995). A large statistical study of the entry of interplanetary magnetic field Y -component into the magnetosphere. *Geophysical Research Letters*, *22*(16), 2083–2086, doi: 10.1029/95GL02261.

Zhang, Y., and L. J. Paxton (2008), An empirical Kp-dependent global auroral model based on TIMED/GUVI FUV data, *J. Atmos. Sol. Terr. Phys*., *70*, 1231–1242, doi:10.1016/j.jastp.2008.03.008.

Zhou, X. W., C. T. Russell, G. Le, S. A. Fuselier, and J. D. Scudder (2000), Solar wind control of the polar cusp at high altitude, *J. Geophys. Res*., *105*, 245.

Zhu, Z., and G. Parks (1993), Particle orbits in model current sheets with a nonzero B_y component, *J. Geophys. Res.*, *98*(A5), 7603–7608, doi: 10.1029/92JA02366.

Figure Caption

Figure 1. Distribution of B_y in the magnetotail associated with IMF penetration for IMF $B_y < 0$. The field-aligned current (red arrows) flows out of the Northern Hemisphere and into the Southern Hemisphere (adopted from Figure 4 of Stenbaek-Nielsen and Otto (1997)).

Figure 2. Distribution of the averaged auroral energy flux in magnetic local time (MLT)-magnetic latitude (MLat) format for (a) Northern Hemisphere and (b) Southern Hemisphere during southward (B_z < -1 nT) interplanetary magnetic field (IMF) and positive *y*-component of IMF (B_y > 2 nT) conditions. (c) and (d) show the number of samples (bins) in NH and SH, respectively, that are used to calculate the averaged energy flux shown in (a) and (b). Two additional constraints are applied to the selection of the samples: |IMF B_x| < 2 nT and SZA > 108°, where SZA is the solar zenith angle.

Figure 3. Same format as Figure 2 but for negative IMF B_y (< -2 nT).

Figure 4. Comparison of hourly sector (≥60° MLat)-averaged auroral energy flux in the (a) Northern Hemisphere and (b) Southern Hemisphere for positive (circle) and negative (filled circle) IMF B_y component. (c) and (d) show comparison of northern and southern hourly sector-averaged auroral energy flux for negative and positive IMF B_y, respectively. The error bars are one standard deviation of the means.

Figure 5. Normalized event distribution of the IMF B_z component for northern hemispheric (blue) and southern hemispheric (red) events shown in Figure 4 for (a) B_y < - 2 nT and (b) B_y > 2 nT.

Figure 6. Liner regression of the averaged auroral energy flux as a function of IMF B_y for (blue) Northern Hemisphere and (red) Southern Hemisphere. The error bars are one-standard deviation of the means. The number of events for each calculated energy flux is plotted on the top panel.

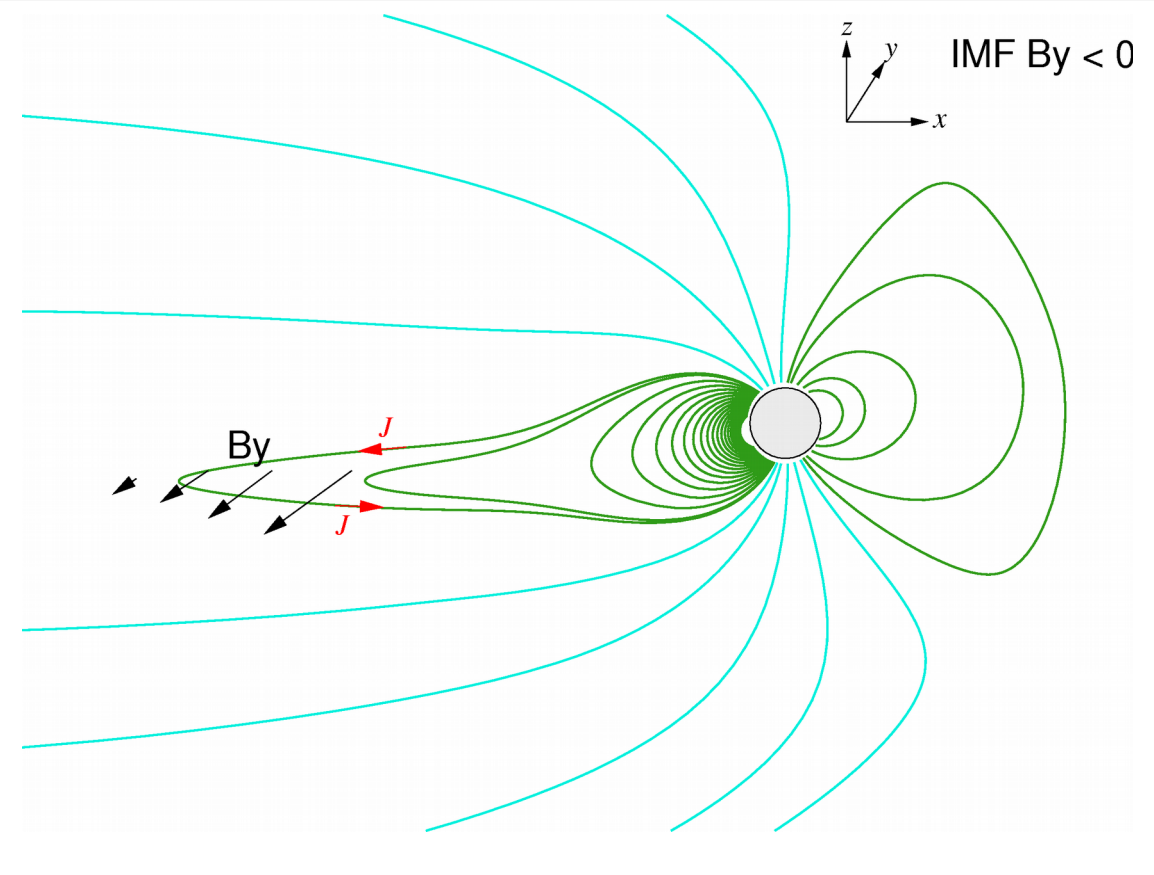

Figure 1. Distribution of B_y in the magnetotail associated with IMF penetration for IMF $B_y < 0$. The field-aligned current (red arrows) flows out of the Northern Hemisphere and into the Southern Hemisphere (adopted from Figure 4 of Stenbaek-Nielsen and Otto (1997)).

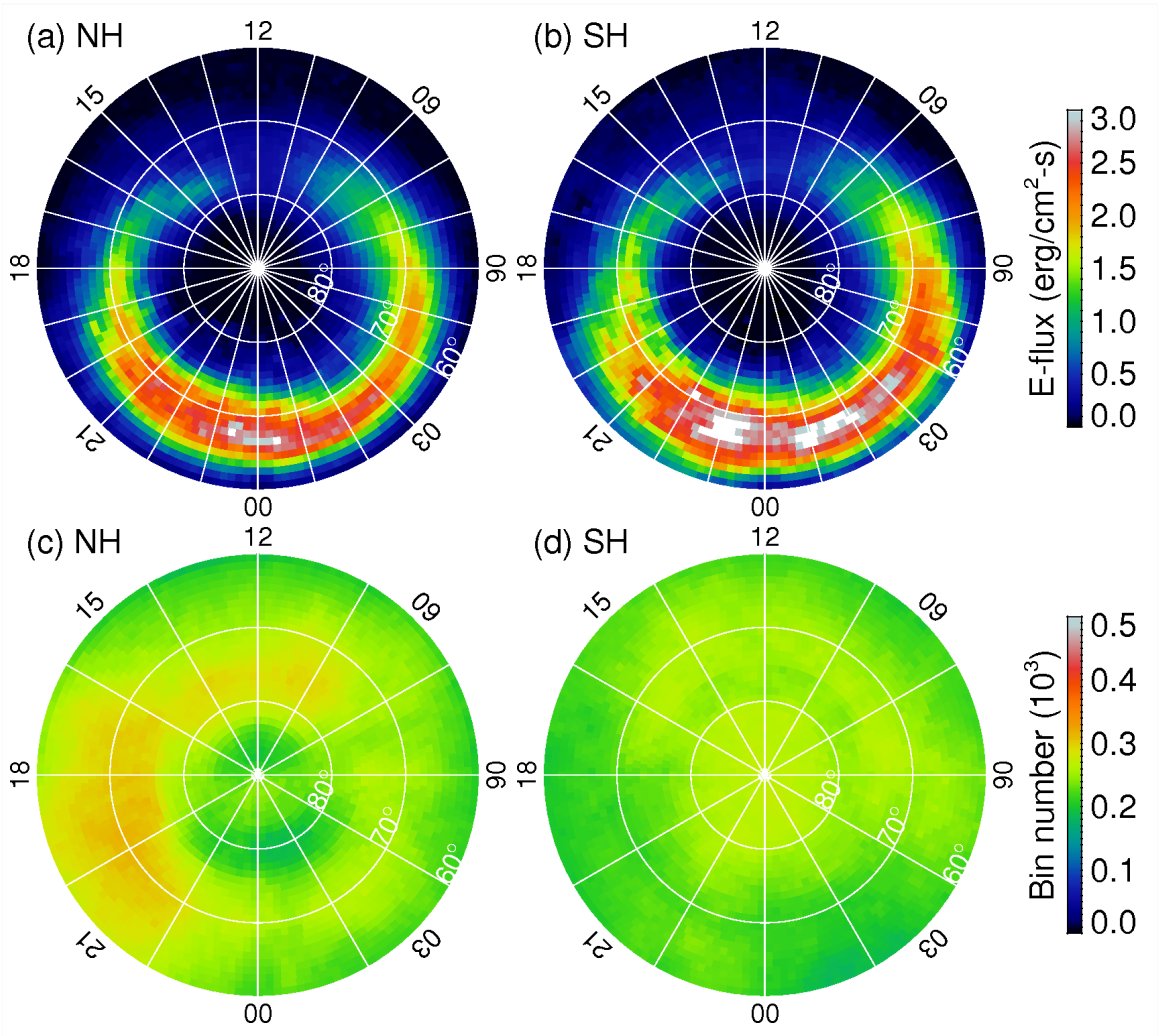

Figure 2. Distribution of the averaged auroral energy flux in magnetic local time (MLT)-magnetic latitude (MLat) format for (a) Northern Hemisphere and (b) Southern Hemisphere during southward (B_z < -1 nT) interplanetary magnetic field (IMF) and positive y-component of IMF (B_y > 2 nT) conditions. (c) and (d) show the number of samples (bins) in NH and SH, respectively, that are used to calculate the averaged energy flux shown in (a) and (b). Two additional constraints are applied to the selection of the samples: |IMF B_x| < 2 nT and SZA > 108°, where SZA is the solar zenith angle.

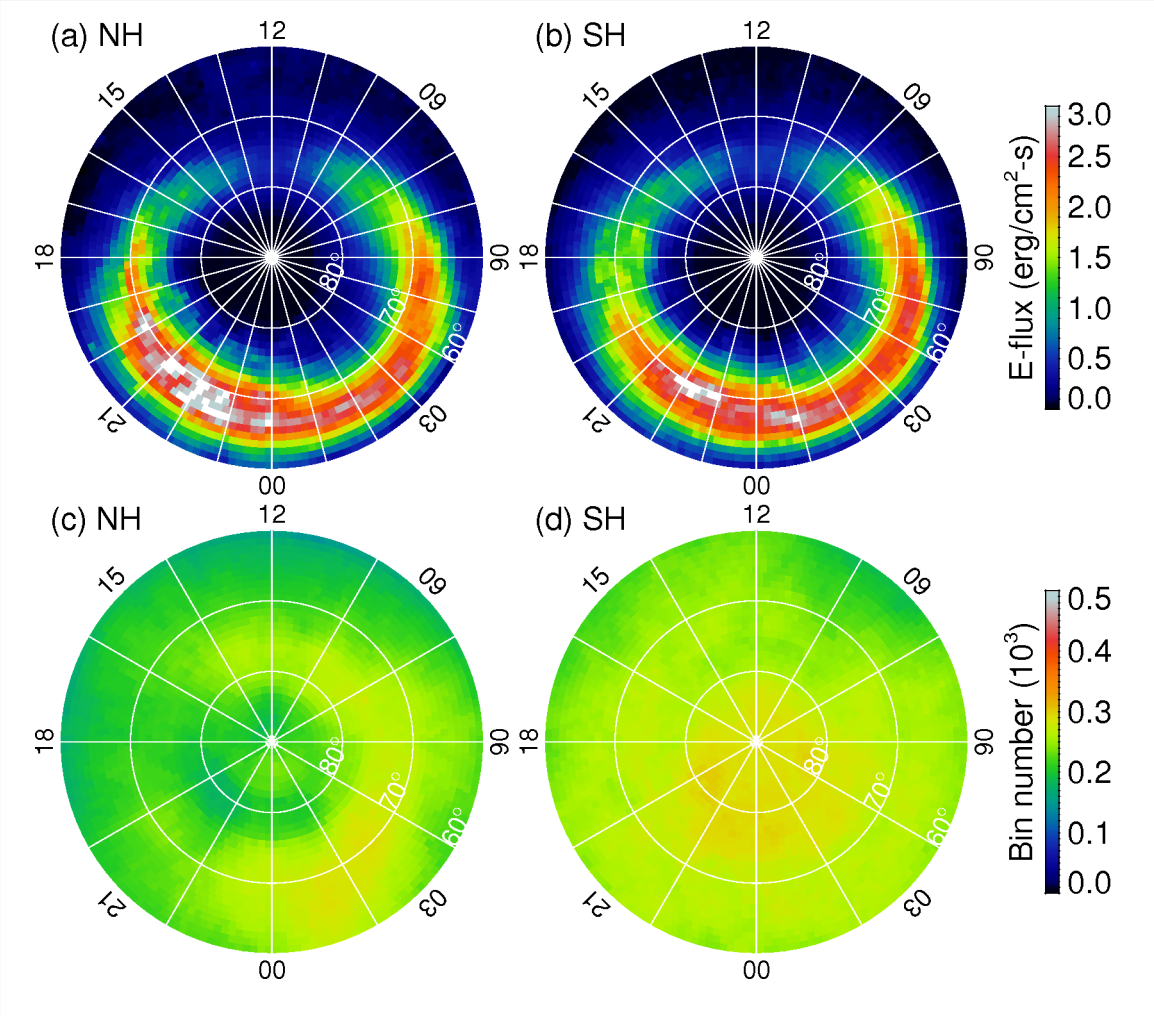

Figure 3. Same format as Figure 2 but for negative IMF B_y (< -2 nT).

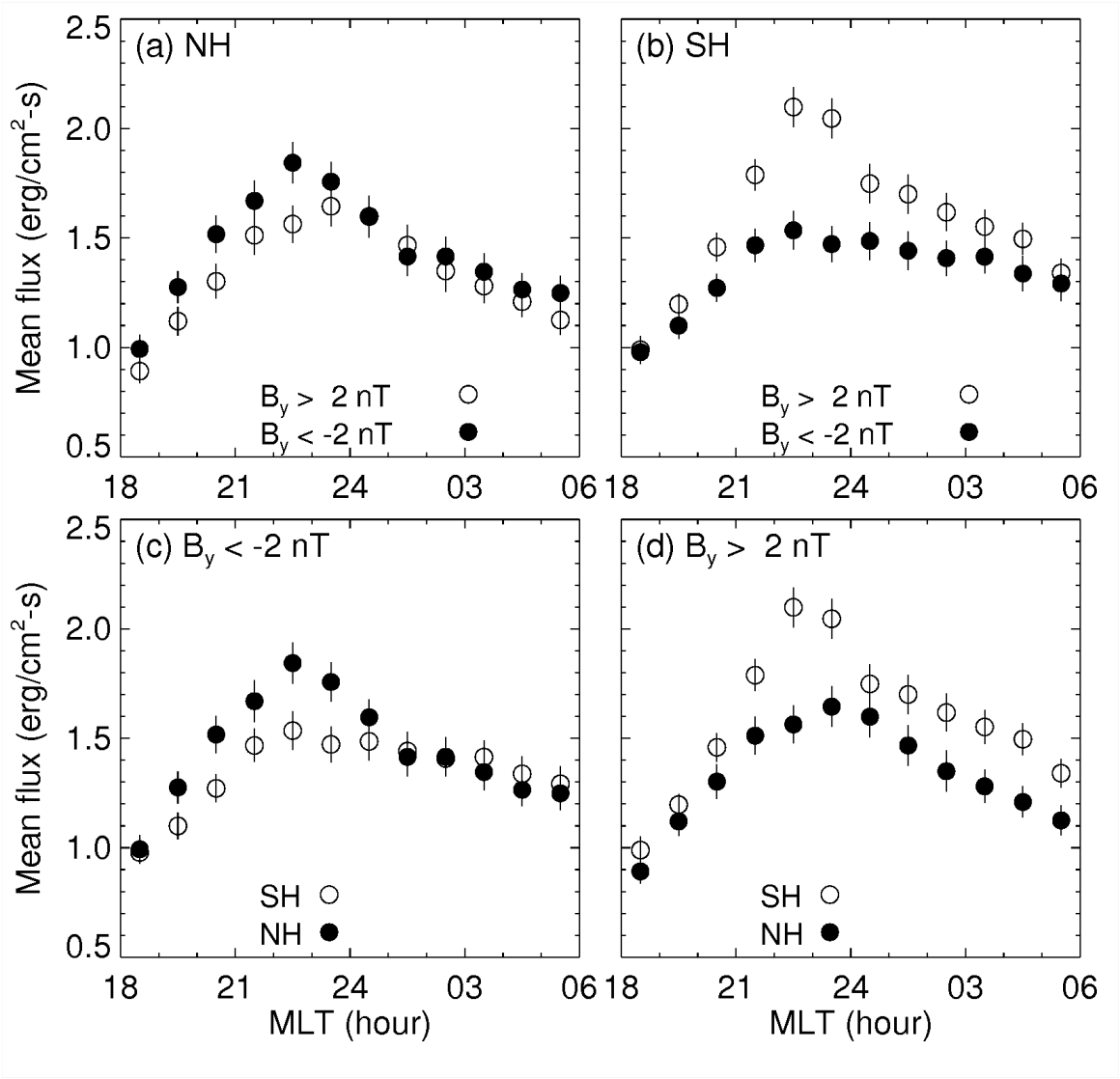

Figure 4. Comparison of hourly sector (≥60° MLat.)-averaged auroral energy flux in the (a) Northern Hemisphere and (b) Southern Hemisphere for positive (circle) and negative (filled circle) IMF B_y component. (c) and (d) show comparison of northern and southern hourly sector-averaged auroral energy flux for negative and positive IMF B_y, respectively. The error bars are one standard deviation of the means.

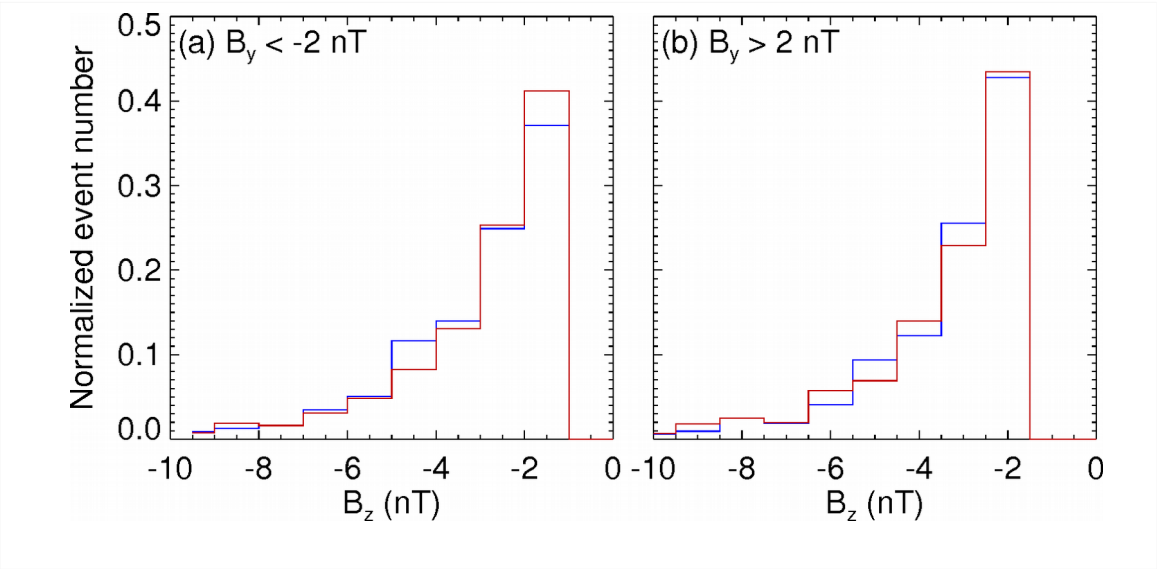

Figure 5. Normalized distribution of the IMF B_z component for northern hemispheric (blue) and southern hemispheric (red) events shown in Figure 4 for (a) B_y < - 2 nT and (b) B_y > 2 nT.

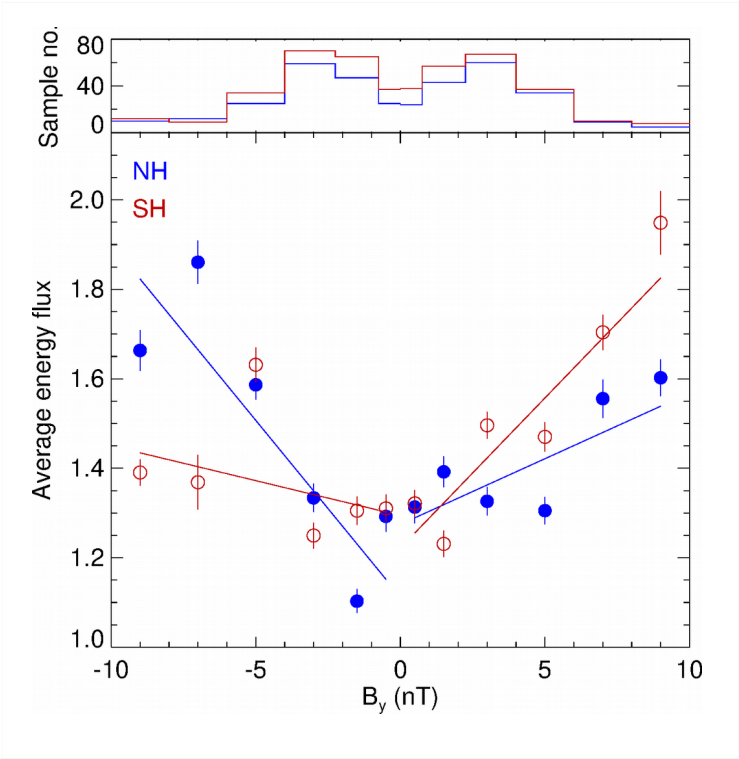

Figure 6. Liner regression of the averaged auroral energy flux as a function of IMF B_y for (blue) Northern Hemisphere and (red) Southern Hemisphere. The error bars are one-standard deviation of the means. The number of events for each calculated energy flux is plotted on the top panel.